Inorg. Chem. **2004**, *43*, 7030–7041

Inorganic Chemistry
Article

Theoretical Investigations of the Electronic Structure and Spectroscopy of Mononuclear, Non-Heme $\{Fe{-}NO\}^6$ Complexes

Shannon N. Greene and Nigel G. J. Richards*

Department of Chemistry, University of Florida, Gainesville, Florida 32611-7200

Received January 6, 2004

The unusual metal coordination and spin-state of the Fe(III) center in nitrile hydratase (NHase) has stimulated the synthesis of numerous model complexes in efforts to understand the reactivity and spectroscopic properties of the enzyme. A particular problem has been the development of model Fe(III) complexes that exhibit reversible, photolabile binding to nitric oxide (NO) in a manner similar to that observed for the NHase metal center. We now report a detailed NBO analysis of the ground-state chemical bonding in three $\{Fe{-}NO\}^6$ complexes that exhibit different responses to irradiation, together with investigations of their spectroscopic properties using semiempirical INDO/S CI singles calculations. Our computational studies reveal a correlation between the photolability of these complexes and the existence of low-energy transitions that promote an electron into the Fe–NO π^* antibonding molecular orbital. In addition to providing detailed insights into how the ligand field influences the spectroscopy of these mononuclear complexes, these studies strengthen our previous conclusions regarding the role of post-translational cysteine modification in modulating the photoreactivity of the inactive, NO complex of NHase.

Introduction

The unusual metal coordination and spin-state of the Fe(III) center in Fe-type nitrile hydratase (NHase),[1-3] which catalyzes the conversion of nitriles to primary amides,[3] has stimulated the synthesis of numerous model complexes in efforts to understand the reactivity and spectroscopy of the enzyme.[4] A particularly interesting feature of Fe-type NHase is the ability of nitric oxide (NO) to interact reversibly with the active site Fe(III),[5] in a process hypothesized to be involved in cellular regulation of the enzyme.[6] Thus, Fe-type NHase activity disappears in vivo due to the formation of a stable Fe−nitrosyl complex when cells containing the enzyme are kept in darkness. Irradiation of NO-inactivated NHase with visible light results in Fe−NO bond cleavage, thereby reactivating the enzyme.[7] The interaction of Fe-type NHase with NO was initially established in an elegant series of photochemical experiments,[5,7] and a detailed picture of how metal-bound NO interacts with protein environment in the nitrosylated enzyme was subsequently provided by high-resolution X-ray crystallography (Figure 1).[1c] The crystal

---

* Corresponding author. E-mail: richards@qtp.ufl.edu.

(1) (a) Tsujimura, M.; Dohmae, N.; Odaka, M.; Chijimatsu, M.; Takio, K.; Yohda, M.; Hoshino, M.; Nagashima, S.; Endo, I. *J. Biol. Chem.* **1997**, *272*, 29454−29459. (b) Huang, W.; Jia, J.; Cummings, J., Nelson, M.; Schneider, G.; Lindqvist, Y. *Structure* **1997**, *5*, 691−699. (c) Nagashima, S.; Nakasako, M.; Dohmae, N.; Tsujimura, M.; Takio, K.; Odaka, M.; Yohda, M.; Kamiya, N.; Endo, I. *Nat. Struct. Biol.* **1998**, *5*, 347−351.

(2) Sugiura, Y.; Kuwahara, J.; Nagasawa, T.; Yamada, H. *J. Am. Chem. Soc.* **1987**, *109*, 5848−5850.

(3) (a) Endo, I.; Nojiri, M.; Tsujimura, M.; Nakasako, M.; Nagashima, S.; Yohda, M.; Odaka, M. *J. Inorg. Biochem.* **2001**, *83*, 247−253. (b) Kobayashi, M.; Shimizu, S. *Curr. Opin. Chem. Biol.* **2000**, *4*, 95−102. (c) Nakasako, M.; Odaka, M.; Yohda, M.; Dohmae, N.; Takio, K.; Kamiya, N.; Endo, I. *Biochemistry* **1999**, *38*, 9887−9898.

(4) (a) Harrop, T. C.; Mascharak, P. K. *Acc. Chem. Res.* **2004**, *37*, 253−260. (b) Kovacs, J. A. *Chem. Rev.* **2004**, *104*, 825−848. (c) Mascharak, P. K. *Coord. Chem. Rev.* **2002**, *225*, 201−214. (d) Marlin, D. S.; Mascharak, P. K. *Chem. Soc. Rev.* **2000**, *29*, 69−74. (e) Artaud, I.; Chatel, S.; Chauvin, A. S.; Bonnet, D.; Kopf, M. A.; Leduc, P. *Coord. Chem. Rev.* **1999**, *190−192*, 577−586.

(5) (a) Odaka, M.; Fujii, K.; Hoshino, M.; Noguchi, T.; Tsujimura, M.; Nagashima, S.; Yohda, M.; Nagamune, T.; Inoue, Y.; Endo, I. *J. Am. Chem. Soc.* **1997**, *119*, 3785−3791. (b) Noguchi, T.; Hoshino, M.; Tsujimura, M.; Odaka, M.; Inoue, Y.; Endo, I. *Biochemistry* **1996**, *35*, 16777−16781.

(6) (a) Endo, I.; Odaka, M. *J. Mol. Catal. B* **2000**, *10*, 81−86. (b) Endo, I.; Odaka, M.; Yohda, M. *Trends Biotechnol.* **1999**, *17*, 244−249. (c) Bonnet, D.; Artaud, I.; Moali, C.; Pétré, D.; Mansuy, D. *FEBS Lett.* **1997**, *409*, 216−220.

(7) (a) Noguchi, T.; Honda, J.; Nagamune, T.; Sasabe, H.; Inoue, Y.; Endo, I. *FEBS Lett.* **1995**, *358*, 9−12. (b) Honda, J.; Kandori, H.; Okada, T.; Nagamune, T.; Shichida, Y.; Sasabe, H.; Endo, I. *Biochemistry* **1994**, *33*, 3577−3583. (c) Honda, J.; Teratani, Y.; Kobayashi, Y.; Nagamune, T.; Sasabe, H.; Hirata, A.; Ambe, F.; Endo, I. *FEBS Lett.* **1992**, *301*, 177−180. (d) Popescu, V.; Munck, E.; Fox, B. G.; Sanakis, Y.; Cummings, J. G.; Turner, I. M.; Nelson, M. J. *Biochemistry* **2001**, *40*, 7984−7991.

10.1021/ic0499695 CCC: $27.50

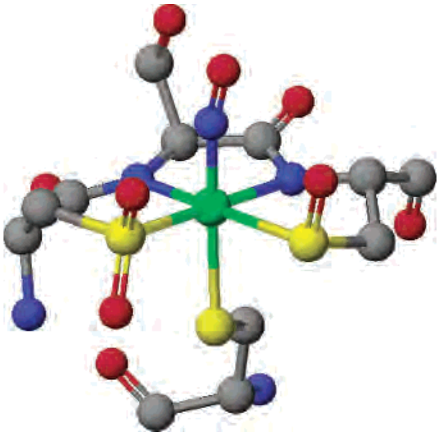

Figure 1. X-ray crystal structure of the metal center in inactive, nitrosylated nitrile hydratase. For clarity, only non-hydrogen atoms are shown, which are colored using the following scheme: C, black; N, blue; O, red; S, yellow; Fe, green. This image was generated using the CACHe Worksystem Pro V6.0 software package.[42]

structure also revealed that the cysteine ligands coordinating the Fe(III) were oxidized as a result of post-translational modification, a transformation that is essential for enzyme activity.[8] The functional role of sulfur oxidation in Fe-type NHase remains the subject of considerable discussion, however, despite the preparation and characterization of many interesting model Fe(III) complexes.[4,9]

The fully reversible inactivation and photochemical reactivation is an intriguing feature of the NO-based regulation of Fe-type NHase because, to our knowledge, only a single model complex has been shown to exhibit similar reversibility in its interaction with NO.[10,11] Indeed, NO prefers to interact with Fe(II) centers,[12] although binding of this small molecule ligand to Fe(III) in a small number of heme and non-heme complexes has been observed.[13] We have proposed that one possible role for post-translational oxidation of two active site cysteines coordinating the metal of Fe-type NHase might be to confer the appropriate photochemical reactivity onto the {Fe−NO}^{6} bond in the inactive form of the enzyme, and have performed theoretical calculations to obtain support for this proposal. Our computational studies suggested that the presence of the sulfinate and sulfenate groups was essential for promotion of an electron into the Fe−NO π^* antibonding molecular orbital (MO) upon the absorption of visible light.[14] On the other hand, since these calculations employed only a gas-phase model of the NHase active site, we have sought to test our conclusions further by calculating the spectroscopic properties of additional NO-containing compounds. While the bonding and reactivity of small molecule Fe−NO complexes have been the subject of computational investigations using a variety of high-level theoretical methods,[15] no such studies of the photolability of these compounds have been reported. We now report theoretical investigations for three {Fe−NO}^{6} complexes (Figure 2), which have been synthesized as models of the Fe center in NHase and exhibit differences in their ability to lose NO upon irradiation.[10,11,13b] For example, complex **1**, in which the metal is coordinated by a deprotonated amide nitrogen,[4d] rapidly releases NO when exposed to light (50 W tungsten lamp) in a process that is completely reversible. Complex **3**, however, does not release NO reproducibly, even upon prolonged irradiation under a variety of conditions,[13a] and while NO is lost when complex **2** is irradiated, the process does not seem to be reversible. This latter finding is presumably because the 5-coordinate intermediate, formed in the photochemical reaction, decomposes under the reported conditions,[11] but no detailed experimental studies of this hypothesis have yet been reported. The computational studies discussed herein reveal a correlation between the photolability of these complexes and the existence of low-energy transitions that promote an electron into the Fe−NO π^* antibonding molecular orbital. These results not only validate the computational strategy that was employed in our previous calculations,[14] thereby providing additional support for the importance of sulfur oxidation in the observed NHase/NO photoreactivity, but yield additional insight into the electronic structure of the {Fe−NO}^{6} complexes **1**−**3** that may underlie their differential photochemical reactivities.

---

(8) (a) Lu, J.; Zheng, Y. J.; Yamagishi, H.; Odaka, M.; Tsujimura, M.; Maeda, M.; Endo, I. *FEBS Lett.* **2003**, *553*, 391−396. (b) Nojiri, M.; Yohda, M.; Odaka, M.; Matsushita, Y.; Tsujimura, M.; Yoshida, T.; Dohmae, N.; Takio, K.; Endo, I. *J. Biochem.(Tokyo)* **1999**, *125*, 696−704. (c) Murakami, T.; Nojiri, M.; Nakayama, H.; Odaka, M.; Yohda, M.; Dohmae, N.; Takio, K.; Nagamune, T.; Endo, I. *Protein Sci.* **2000**, *9*, 1024−1030.

(9) (a) Galardon, E.; Giorgi, M.; Artaud, I. *Chem. Commun.* **2004**, 286−287. (b) Lee, C.-M.; Hsieh, C.-H.; Dutta, A.; Lee, G.-H.; Liaw, W.-F. *J. Am. Chem. Soc.* **2003**, *125*, 11492−11493. (c) Tyler, L. A.; Noveron, J. C.; Olmstead, M. M.; Mascharak, P. K. *Inorg. Chem.* **1999**, *38*, 616−617.

(10) (a) Patra, A. K.; Afshar, R.; Olmstead, M. M.; Mascharak, P. K. *Angew. Chem., Int. Ed. Engl.* **2002**, *41*, 2512−2515. (b) Patra, A. K.; Rowland, J. M.; Marlin, D. S.; Bill, E.; Olmstead, M. M.; Mascharak, P. K. *Inorg. Chem.* **2003**, *42*, 6812−6823.

(11) Schweitzer, D.; Ellison, J. J.; Shoner, S. C.; Lovell, S.; Kovacs, J. A. *J. Am. Chem. Soc.* **1998**, *120*, 10996−10997.

(12) (a) McCleverty, J. A. *Chem. Rev.* **2004**, *104*, 403−418. (b) Ford, P. C.; Laverman, L. E.; Lorkovic, I. M. *Adv. Inorg. Chem.* **2003**, *54*, 203−257. (c) Butler, A. R.; Megson, I. L. *Chem. Rev.* **2002**, *102*, 1155−1165. (d) Westcott, B. L.; Enemark, J. H. In *Inorganic Electronic Structure and Spectroscopy*; Solomon, E. I.; Lever, B. P., Eds.; Wiley-Interscience: New York, 1999; Vol. II, pp 403−450. (e) Enemark, J. H.; Feltham, R. D. *Coord. Chem. Rev.* **1974**, *13*, 339−406.

(13) (a) Grapperhaus, C. A.; Li, M.; Patra, A. K.; Poturovic, S.; Kozlowski, P. M.; Zgierski, M. Z.; Mashuta, M. S. *Inorg. Chem.* **2003**, *42*, 4382−4388. (b) Grapperhaus, C. A.; Patra, A. K.; Mashuta, M. S. *Inorg. Chem.* **2002**, *41*, 1039−1041. (c) Hauser, C.; Glaser, T.; Bill, E.; Weyhermüller, T.; Wieghardt, K. *J. Am. Chem. Soc.* **2000**, *122*, 4352−4364. (d) Ellison, M. K.; Scheidt, W. R. *J. Am. Chem. Soc.* **1999**, *121*, 5210−5219. (e) Scheidt, W. R.; Lee, Y. J.; Hatano, K. *J. Am. Chem. Soc.* **1984**, *106*, 3191−3198.

(14) Greene, S. N.; Chang, C. H.; Richards, N. G. J. *Chem. Commun.* **2002**, 2386−2387.

(15) (a) Andrews, L.; Citra, A. *Chem. Rev.* **2002**, *102*, 885−912. (b) Jackson, T. A.; Yikilmaz, E.; Miller, A.-F.; Brunold, T. C. *J. Am. Chem. Soc.* **2003**, *125*, 8348−8363. (c) Zhang, Y.; Gossman, W.; Oldfield, E. *J. Am. Chem. Soc.* **2003**, *125*, 16387−16396. (d) Boulet, P.; Buchs M.; Chermette, H.; Daul, C.; Gilardoni, F.; Rogemond, F.; Schläpfer, C. W.; Weber, J. *J. Phys. Chem. A* **2001**, *105*, 8991−8998. (e) Gonzalez Lebrero, M. C.; Scherlis, D. A.; Estiú, G. L.; Olabe, J. A.; Estrin, D. A. *Inorg. Chem.* **2001**, *40*, 4127−4133. (f) Wanner, M.; Scheiring, T.; Kaim, W.; Slep, L. D.; Baraldo, L. M.; Olabe, J. A.; Zális, S.; Baerends, E. J. *Inorg. Chem.* **2001**, *40*, 5704−5707. (g) Scherlis, D. A.; Cymeryng, C. B.; Estrin, D. A. *Inorg. Chem.* **2000**, *39*, 2352−2359. (h) Brown, C. A.; Pavlovsky, M. A.; Westre, T. E.; Zhang, Y.; Hedman, B.; Hodgson, K. O.; Solomon E. I. *J. Am. Chem. Soc.* **1995**, *117*, 715−732.

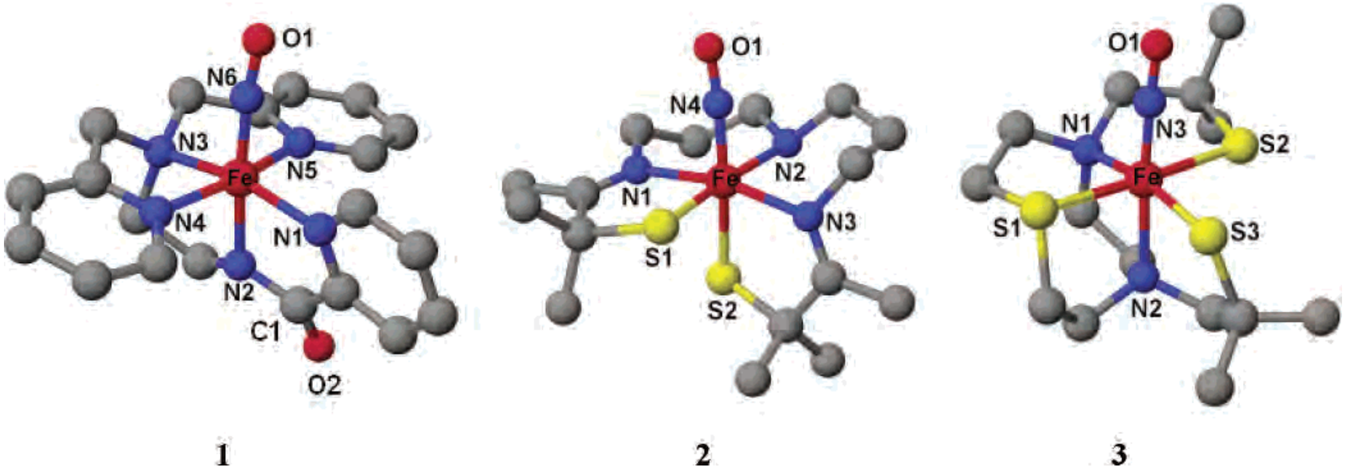

1 **2** **3**

Figure 2. X-ray crystal structures of $\{Fe{-}NO\}^6$ complexes **1**−**3**: **1**, [*N*-[2-[bis[(2-pyridinyl-κ)methyl]amino-κN]ethyl]-2-pyridinecarboxamidato-κN1, κN2]-nitrosyliron(II);[10] **2**, [[3,3′-[(imino-κN)bis(3,1-propanediylnitrilo-κN)]bis[2-methyl-2-butanethiolato-κS]]nitrosyliron(II);[11] **3**, [hexahydro-$\alpha,\alpha,\alpha',\alpha'$-tetra-methyl-1,4,7-thiadiazonine-4,7-diethanethiolato-κN4,κ N7,κS1,κS4,κS7]nitrosyliron(II).[15b] In the coordinate systems for these complexes, the *z*-axis was placed along the $Fe{-}N_{NO}$ bond, with the *x*-axis being defined by one of the equatorial metal−ligand bonds. For clarity, we show only non-hydrogen atoms, which are colored using the following scheme: C, black; N, blue; O, red; S, yellow; Fe, orange. This image was generated using the CAChe Worksystem Pro V6.0 software package.[42]

Computational Methodology

Atomic coordinates for complexes **1**−**3** (Figure 2)[10,11,13b] were obtained from the Cambridge Crystallographic Database.[16] Explicit solvent molecules and counterions were not included in any of the calculations. Optimized structures of all three complexes were obtained using the BLYP exchange-correlation functional[17,18] and were computed with the TURBOMOLE software package.[19] Single point energies were then calculated for the molecules at their optimized geometries with B3LYP[20,21] as implemented in Gaussian98,[22] which uses the third form of the VWN local correlation functional (VWN-III).[23] All calculations employed a 6-31G* basis,[24] although polarization functions were not included on carbon atoms. This choice of basis has been shown to give excellent geometries and electronic structures for related, non-heme Fe(III) complexes with N/S coordination.[25] The density matrix in all single point energy calculations was converged to a tight root mean square threshold of 10^{-8} au, and geometry optimizations were converged to a gradient of 10^{-3} hartree/bohr. To assess the accuracy of these BLYP-derived structures, complex **1** was also optimized using the B3LYP functional with a 6-31G* basis lacking polarization functions on carbon. The converged BLYP molecular orbital coefficients were employed as initial guesses for all B3LYP computations on complexes **1**−**3**. We note that B3LYP has been demonstrated to give reliable transition metal geometries.[26] The chemical bonding in each of the three $\{Fe{-}NO\}^6$ complexes at their BLYP-optimized ground-state geometries was evaluated by natural bond orbital (NBO) analysis[27] of the appropriate density matrix obtained from B3LYP single point calculations. Quantitative analyses of the NBOs and their corresponding natural localized molecular orbitals (NLMOs) to estimate bond covalencies were performed using the approach that we have described for open-shell Fe(III) complexes,[25] except that the population of antibonding orbitals was considered where appropriate. All NBO studies were carried out with the NBO 5.0 software package.[28]

Electronic transition energies and oscillator strengths were calculated for complexes **1**−**3** at their BLYP-optimized, gas-phase geometries using the semiempirical INDO/S CI singles (CIS)

---

(16) Allen, F. H.; Bellard, S.; Brice, M. D.; Cartwright, B. A.; Doubleday: A.; Higgs, H.; Hummelink, T.; Hummelink-Peters, B. G.; Kennard, O.; Motherwell, W. D. S.; Rodgers, J. R.; Watson, D. G. *Acta Crystallogr. Sect. B* **1979**, *35*, 2331−2339.

(17) Becke, A. D. *Phys. Rev. A* **1988**, *38*, 3098−3100.

(18) Lee, C.; Yang, W.; Parr, R. G. *Phys. Rev. B* **1988**, *37*, 785−789.

(19) (a) Von Arnim, M.; Ahlrichs, R. *J. Comput. Chem.* **1998**, *19*, 1746−1757. (b) Ahlrichs, R.; Bär, M.; Häser, M.; Horn, H.; Kölmel, C. *Chem. Phys. Lett.* **1989**, *162*, 165−169.

(20) Becke, A. D. *J. Chem. Phys.* **1993**, *98*, 5648−5652.

(21) Stephens, P. J.; Devlin, F. J.; Chabalowski, C. F.; Frisch, M. J. *J. Phys. Chem.* **1994**, *98*, 11623−11627.

(22) Frisch, M. J.; Trucks, G. W.; Schlegel, H. B.; Scuseria, G. E.; Robb, M. A.; Cheeseman, J. R.; Zakrzewski, V. G.; Montgomery, J. A., Jr.; Stratmann, R. E.; Burant, J. C.; Dapprich, S.; Millam, J. M.; Daniels, A. D.; Kudin, K. N.; Strain, M. C.; Farkas, O.; Tomasi, J.; Barone, V.; Cossi, M.; Cammi, R.; Mennucci, B.; Pomelli, C.; Adamo, C.; Clifford, S.; Ochterski, J.; Petersson, G. A.; Ayala, P. Y.; Cui, Q.; Morokuma, K.; Malick, D. K.; Rabuck, A. D.; Raghavachari, K.; Foresman, J. B.; Cioslowski, J.; Ortiz, J. V.; Baboul, A. G.; Stefanov, B. B.; Liu, G.; Liashenko, A.; Piskorz, P.; Komaromi, I.; Gomperts, R.; Martin, R. L.; Fox, D. J.; Keith, T.; Al-Laham, M. A.; Peng, C. Y.; Nanayakkara, A.; Gonzalez, C.; Challacombe, M.; Gill, P. M. W.; Johnson, B. G.; Chen, W.; Wong, M. W.; Andres, J. L.; Gonzalez, C.; Head-Gordon, M.; Replogle, E. S.; Pople, J. A. *Gaussian 98*, Revision A.7; Pittsburgh, PA, 1998.

(23) Vosko, S. H.; Wilk, L.; Nusair, M. *Can. J. Phys.* **1980**, *58*, 1200−1211.

(24) (a) Hehre, W. J.; Ditchfield, R.; Pople, J. A. *J. Chem. Phys.* **1972**, *56*, 2257−2261. (b) Hariharan, P. C.; Pople, J. A. *Theor. Chim. Acta* **1973**, *28*, 213−222. (c) Francl, M. M.; Pietro, W. J.; Hehre, W. J.; Binkley, J. S.; Gordon, M. S.; DeFrees, D. J.; Pople, J. A. *J. Chem. Phys.* **1982**, *77*, 3654−3665. (d) Rassolov, V.; Pople, J. A.; Ratner, M. A.; Windus, T. L. *J. Chem. Phys.* **1998**, *109*, 1223−1229. (e) Feller, D.; Davidson, E. R. In *Reviews in Computational Chemistry;* Lipkowitz, K. B.; Boyd, D. B., Eds.; VCH: New York, 1990; Vol. 1, pp 1−43.

(25) (a) Chang, C. H.; Boone, A. J.; Bartlett, R. J.; Richards, N. G. J. *Inorg. Chem.* **2004**, *43*, 458−472. (b) Boone, A. J.; Chang, C. H.; Greene, S. N.; Herz, T.; Richards, N. G. J. *Coord. Chem. Rev.* **2003**, *238−239*, 291−314.

(26) (a) Siegbahn, P. E. M. *Adv. Chem. Phys.* **1996**, *93*, 333−387. (b) Siegbahn, P. E. M.; Blomberg, M. R. A. *Chem. Rev.* **2000**, *100*, 421−437. (c) Siegbahn, P. E. M.; Blomberg, M. R. A. *Annu. Rev. Phys. Chem.* **1999**, *50*, 221−249.

(27) (a) Reed, A. E.; Curtiss, L. A.; Weinhold, F. *Chem. Rev.* **1988**, *88*, 899−926. (b) Weinhold, F. In *Encyclopedia of Computational Chemistry*; Schleyer, P. v. R.; Allinger, N. L.; Clark, T.; Gasteiger, J.; Kollman, P. A.; Schaefer, H. F., III; Schreiner, P. R., Eds.; Wiley: Chichester, 1998; pp 1792−1811.

(28) Glendening, E. D.; Badenhoop, J. K.; Reed, A. E.; Carpenter, J. E.; Bohmann, J. A.; Morales, C. M.; Weinhold, F. *NBO 5.0*. Theoretical Chemistry Institute, University of Wisconsin: Madison, WI, 2001.

approximation.[29,30] All INDO/S calculations employed a β_d value of -23.0 eV for iron[29a] and standard resonance integrals and interaction factors ($f_{p\sigma p\sigma} = 1.267$ and $f_{p\pi p\pi} = 0.585$).[29b,29c] The CIS calculation for each model included singly excited configurations from a RHF ground state reference determinant. The CI active spaces for INDO/S studies were chosen on the basis of an initial CI using an active space composed of all occupied, heavy-atom valence MOs excited into all virtual MOs of lower energy than that of the MO composed principally of the Fe 4p orbitals. Orbitals comprising the active space were then selected on the basis of configurations that had energies within 50 000 cm^{-1} of the ground state in this initial CI calculation. Although this yielded relatively small active spaces for the three $\{Fe-NO\}^6$ complexes in this study, using larger active spaces gave much poorer agreement between experimental and calculated spectra, presumably due to limitations within the INDO approximation.[31,32] INDO/S CIS calculations that included the effects of solvent environment employed a self-consistent reaction field (SCRF) model, which has been described in detail elsewhere.[33] The CI active spaces for these INDO/S-SCRF calculations were chosen using the same procedure as described for the in vacuo studies. All calculated absorption energies and oscillator strengths were fit to normalized Gaussian functions with bandwidths of 3200 cm^{-1} in order to facilitate comparison of theoretical and experimental spectra. Similar fitting procedures have been used in theoretical studies of other iron complexes.[34]

Results and Discussion

Electronic Structure and Ground-State Bonding of Fe(III) Complexes 1−3. In many respects, the DFT-optimized and experimental structures for complexes **1**−**3** (Figure 2) were very similar, as judged by comparison of bond lengths and bond angles, although deviations between theory and experiment were observed for some dihedral angles in complex **1** (Table 1). For example, the Fe−N2−C1−O1 dihedral angle of the amide ligand was less planar in the crystal structure than the in vacuo theoretical geometry. The deviation from planarity in the experimental structure is, however, likely associated with crystal packing effects rather than deficiencies in the computational approach (see Supporting Information). Control calculations using complex **1** established that there was little difference between BLYP- and B3LYP-optimized geometries, justifying our use of the less computationally demanding BLYP functional to obtain in vacuo optimized structures for the remaining complexes. In all of the complexes, the Fe−NO bond length was significantly shorter than all other Fe−ligand bonds, consistent with a greater ground-state bond order between the nitrosyl ligand and the metal in these $\{Fe-NO\}^6$ complexes.[12] The calculated Fe−N−O bond angle varied from 172° to 177°, these values being well within the typical range observed for $\{Fe-NO\}^6$ complexes.[12d]

Table 1. Selected Structural Properties of the Crystal and the DFT-Optimized Geometries for $\{Fe-NO\}^6$ Complexes **1**−**3**[a]

internal coordinate	crystal structure[b]	BLYP/6-31G*	B3LYP/6-31G*
	Complex **1**		
Fe−N1	1.978(2)	2.02	2.01
Fe−N2	1.9009(19)	1.90	1.88
Fe−N3	1.972(2)	2.03	2.01
Fe−N4	1.982(2)	2.04	2.02
Fe−N5	1.983(2)	2.03	2.02
Fe−N6	1.677(2)	1.68	1.66
N6−O1	1.139(3)	1.17	1.15
Fe−N6−O1	173.1(2)	170.0	169.9
Fe−N2−C1−O2	155.4	171.7	170.1
	Complex **2**		
Fe−N1	1.993(3)	2.03	*c*
Fe−N2	2.108(3)	2.16	*c*
Fe−N3	1.979(3)	1.99	*c*
Fe−N4	1.676(3)	1.66	*c*
Fe−S1	2.2603(9)	2.33	*c*
Fe−S2	2.2604(9)	2.30	*c*
N4−O1	1.161(4)	1.18	*c*
Fe−N4−O1	172.3(3)	172.6	*c*
	Complex **3**		
Fe−S1	2.285(2)	2.37	*c*
Fe−S2	2.284(2)	2.33	*c*
Fe−S3	2.291(2)	2.34	*c*
Fe−N1	2.024(5)	2.08	*c*
Fe−N2	2.063(5)	2.13	*c*
Fe−N3	1.609(6)	1.62	*c*
N3−O1	1.167(6)	1.17	*c*
Fe−N3−O1	177.2(6)	177.0	*c*

[a] Atom labels correspond to those shown in Figure 2. [b] All bond distances and angles are reported in units of Å and degrees, respectively. Values in parentheses are the errors reported for the experimental measurements. [c] Calculation was not performed.

A detailed analysis of the Kohn−Sham wave function was undertaken to determine the bonding between the metal and the NO ligand in these $\{Fe-NO\}^6$ complexes, since the species $[Fe(II)-NO^+]$, $[Fe(III)-NO\bullet]$, or $[Fe(IV)-NO^-]$ can all give rise to an $S = 0$ spin state. Hence, the B3LYP first-order reduced density matrix was obtained in both a restricted and unrestricted formalism for complexes **1**−**3** at their BLYP-optimized geometries. While there was no difference between the restricted and unrestricted B3LYP wave functions for complexes **1** and **2** (i.e., all electrons were perfectly paired with an orbital overlap of unity so that $S = 0$, and both calculations gave an identical total energy), this proved not to be the case for complex **3** (vide infra). NBO analysis[27] was therefore carried out on the restricted B3LYP density matrixes for complexes **1** and **2** and on the unrestricted B3LYP density matrix in the case of complex **3**. NBOs were

---

(29) (a) Zerner, M. C.; Loew, G. H.; Kirchner, R. F.; Mueller-Westerhoff, U. T. *J. Am. Chem. Soc.* **1980**, *102*, 589−599. (b) Bacon, A. D.; Zerner, M. C. *Theor. Chim. Acta* **1979**, *53*, 21−54. (c) Ridley, J.; Zerner, M. *Theor. Chim. Acta* **1973**, *32*, 111−134. (d) Zerner, M. C. In *Reviews in Computational Chemistry*; Lipkowitz, K. B.; Boyd, D. B., Eds.; VCH: New York, 1991; Vol. 2, pp 313−365.

(30) All INDO/S calculations were performed using in-house software packages at the Quantum Theory Project, University of Florida.

(31) (a) Bunce, N. J.; Ridley, J. E.; Zerner, M. C. *Theor. Chim. Acta* **1977**, *45*, 283−300. (b) Loew, G. H.; Herman, Z. S.; Zerner, M. C. *Int. J. Quantum Chem.* **1980**, *18*, 481−492. (c) Zerner, M. *J. Chem. Phys.* **1975**, *62*, 2788−2799.

(32) The lack of including explicit overlap between orbitals located on different atoms in the INDO/S model has the effect at the SCF level of inappropriately lowering the energy of the σ MOs. Therefore, the inclusion of these MOs, and their virtual counterparts, in any subsequent CIS calculation does not necessarily give calculated spectra that are in better agreement with experiment. The best results are obtained with a “balanced” active space that models the character of the ground and excited states.[29]

(33) (a) Karelson, M. M.; Zerner, M. C. *J. Phys. Chem.* **1992**, *96*, 6949−6957. (b) Szafran, M.; Karelson, M. M.; Katritzky, A. R.; Koput, J.; Zerner, M. C. *J. Comput. Chem.* **1993**, *14*, 371−377. (c) Hush, N. S.; Reimers, J. R. *Chem. Rev.* **2000**, *100*, 775−786.

(34) (a) Kotzian, M.; Rösch, N.; Schröder, H.; Zerner, M. C. *J. Am. Chem. Soc.* **1989**, *111*, 7687−7696. (b) Loew, G. H.; Harris, D. L. *Chem. Rev.* **2000**, *100*, 407−419. (c) Cory, M. G.; Stavrev, K. K.; Zerner, M. C. *Int. J. Quantum Chem.* **1997**, *63*, 781−795.

Table 2. NPA-Derived Partial Charges of Selected Atoms in $\{Fe{-}NO\}^6$ Complexes **1**−**3** at Their DFT-Optimized Geometries[a,b]

complex **1**		complex **2**		complex **3**		
atom	partial charge	atom	partial charge	atom	partial charge	spin density
Fe	+1.39	Fe	+1.25	Fe	+1.17	+0.308
N1	−0.55	N1	−0.54	N1	−0.54	−0.004
N2	−0.67	N2	−0.73	N2	−0.55	−0.005
N3	−0.52	N3	−0.55	N3	+0.11	−0.123
N4	−0.53	N4	+0.06	S1	+0.32	−0.005
N5	−0.53	S1	−0.22	S2	−0.26	−0.031
N6	+0.10	S2	−0.29	S3	−0.26	−0.016
O1	−0.09	O1	−0.16	O1	−0.13	−0.120
O2	−0.54					

[a] Atom labels correspond to those shown in Figure 2. [b] Spin densities for complex **3** are computed from the unrestricted B3LYP wave function, and positive values are arbitrarily assigned to β spin density.

Table 3. Selected NLMO/NPA and NBO Bond Orders in $\{Fe{-}NO\}^6$ Complexes **1**−**3** at Their BLYP-Optimized Geometries Computed from the Appropriate B3LYP/6-31G* Density Matrix[a]

bond	NLMO/NPA	NBO	bond	NLMO/NPA	NBO
		Complex **1**			
Fe−N1	0.171	*b*	Fe−N6	1.238	1.375
Fe−N2	0.463	*b*	N6−O1[c]	1.499	0.988
Fe−N3	0.197	*b*	N2−C1	0.907	0.944
Fe−N4	0.269	*b*	C1−O2	1.319	1.814
Fe−N5	0.234	*b*			
		Complex **2**			
Fe−N1	0.180	*b*	Fe−S1	0.649	0.817
Fe−N2	0.114	*b*	Fe−S2	0.578	0.800
Fe−N3	0.214	*b*	N4−O2[c]	1.428	0.976
Fe−N4	1.351	1.370			
		Complex **3**			
Fe−S1	0.206	*b*	Fe−N2	0.138	*b*
Fe−S2	0.585	0.799	Fe−N3	1.175	1.020
Fe−S3	0.683	0.804	N3−O1[c]	1.634	1.353
Fe−N1	0.147	*b*			

[a] Atom labels correspond to those shown in Figure 2. [b] Bond orders are lower than the default threshold chosen to define an NBO. [c] The corresponding NLMO/NPA and NBO bond orders for free NO are both 2.5.

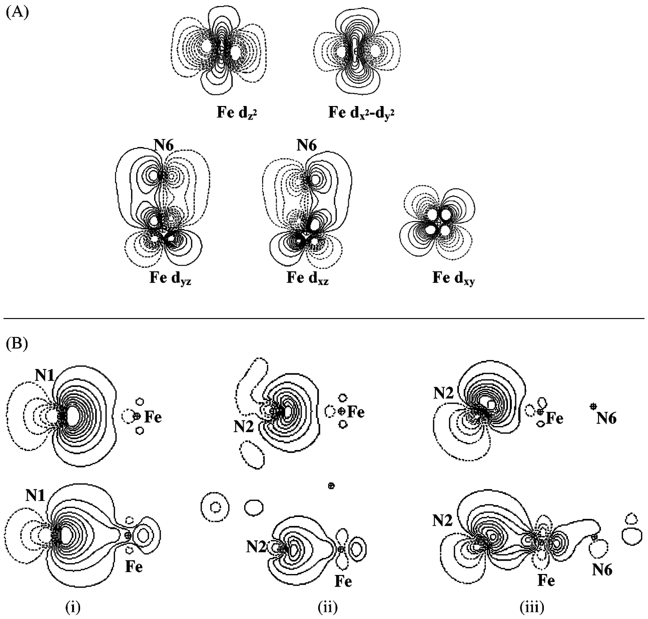

Figure 3. (A) NBOs with significant Fe character in complex **1**, corresponding to three doubly occupied Fe d orbitals (bottom) and two unoccupied orbitals (top). (B) Selected NBOs (top) and their corresponding NLMOs (bottom) demonstrating ligand-to-metal σ donation between Fe and pyridine (i) or carboxamido (ii, iii) nitrogen donors in complex **1**. Atom labels, which indicate the nuclei associated with the electrons in the MO, correspond to those shown in Figure 2, and all contour plots were generated with NBOView 1.0 using a value of 0.03.[43]

compared to their corresponding NLMOs in order to gain more detailed insight into the different symmetries of metal−ligand interactions, using methods that we have described previously,[25a] and bond covalencies were calculated on the basis of the number of shared electrons.

Although the metal center in all three complexes possesses a formal oxidation state of +3, the partial charges computed using natural population analyses (NPA) are substantially lower, suggesting donation of electron density from the ligands to the metal center (Table 2). We note that the larger amount of positive charge on Fe in complex **1** relative to that computed for **3** is in agreement with expectations based on the atomic polarizabilities of sulfur and nitrogen. Thus, the partial positive charge associated with the Fe center should decrease with an increasing ratio of sulfur to nitrogen ligands, given that sulfur is a more polarizable ligand than nitrogen. This observation is also consistent with the NPA partial charges computed for the sulfur and non-NO nitrogen ligands in complexes **1**−**3** (Table 2).

The extent of covalency in the $Fe{-}N_{NO}$ bonds in the three $\{Fe{-}NO\}^6$ complexes was computed using the preorthogonal natural atomic orbital (pNAO) compositions of localized molecular orbitals, with the sign of these values being obtained from the overlap integrals between hybrid orbitals located on the covalently bonded atoms (Table 3). Such bond orders have been considered to be superior to alternative metrics,[27b] and have been applied in analyses of the extent of d-orbital participation in the bonding of main-group complexes.[35] This analysis revealed that the $Fe{-}N_{NO}$ bond in complex **1** possesses double bond character, as indicated by (i) the calculated NLMO/NPA and NBO bond orders of 1.238 and 1.375, respectively (Table 3), and (ii) the two doubly occupied bonding NBOs between Fe and NO (see Table S1 in the Supporting Information). Inspection of natural hybrid orbital (NHO) compositions and occupancies suggests that the bonding between Fe and the nitrogen of the NO ligand is of π symmetry, consisting of approximately 63% Fe (d_{yz} and d_{xz}) and 27% NO π^* character. This Fe−NO bonding is strikingly similar to that reported in recent calculations on another $\{FeNO\}^6$ complex, which possesses a related coordination sphere.[36] In terms of orbital occupation, there are three doubly occupied Fe orbitals (Figure 3A) and an empty NO π^* orbital, suggesting that complex **1** may be best regarded formally as an Fe(II) d^6 low-spin system bonded to NO^+. The existence of π-back-bonding between Fe(II) and NO^+ is, however, evident from the NO π^* character in the Fe d-orbitals (Figure 3A)[36] and the NPA-

---

(35) Reed, A. E.; Schleyer, P. v. R. *J. Am. Chem. Soc.* **1990**, *112*, 1434−1445.

(36) Serres, R. G.; Grapperhaus, C. A.; Bothe, E.; Bill, E.; Weyhermüller, T.; Neese, F.; Wieghardt, K. *J. Am. Chem. Soc.* **2004**, *126*, 5138−5153.

Table 4. Calculated Covalent Character of Fe−Ligand Bonds in $\{Fe{-}NO\}^6$ Complexes **1**−**3** at Their BLYP-Optimized Ground State Geometries[a]

complex **1**			complex **2**			complex **3**		
	covalency ($\|e^-\|$)			covalency ($\|e^-\|$)			covalency ($\|e^-\|$)	
bond	bond	total	bond	bond	total	bond	bond	total
Fe−N1	0.187	3.804	Fe−N1	0.182	5.283	Fe−S1	0.179	5.083
Fe−N2	0.402		Fe−N2	0.109		Fe−S2	1.064	
Fe−N3	0.216		Fe−N3	0.224		Fe−S3	1.110	
Fe−N4	0.230		Fe−N4	2.769		Fe−N1	0.119	
Fe−N5	0.194		Fe−S1	1.080		Fe−N2	0.139	
Fe−N6	2.575		Fe−S2	0.949		Fe−N3	2.472	

[a] Atom labels correspond to those shown in Figure 2.

derived partial charge for the NO moiety of −0.01 $|e^-|$. From the analysis of pure NBOs, the formal N−O bond order in *free* NO is 2.5, neglecting any lone pair contributions to covalency. Comparison of the NBOs describing free NO and the NO ligand in complex **1** shows a calculated decrease of approximately 1.5 in the N−O bond order (Table 3), consistent with weakening of this bond when the ligand binds to the metal center. On the basis of our NBO analysis, we conclude that NO donates its unpaired π^* electron to the metal, giving filled d_{xy}, d_{xz}, and d_{yz} orbitals, and the latter transfer electron density into two p-orbitals on the nitrogen atom of NO. In addition, electrons that are usually shared in the N−O π-bond become localized as an oxygen lone pair in the bound ligand (Figure 3A). While the bonding between Fe and NO therefore involves two bonds of π-symmetry, the bonds between Fe and the remaining nitrogen ligands arise from σ-donation (Figure 3B). It has been proposed that coordination of Fe by the carboxamido moiety in **1** is important for the observed photolability of this complex.[4d,10] Although recognizing that ground-state bonding is not necessarily relevant to excited-state properties such as photolability, our NBO analysis does suggest that (i) the relevant Fe−N2 bond (Figure 2) has the most covalent character of the five Fe−N bonds that do not involve the NO ligand and (ii) there is very little covalency in the bonding between Fe and the nitrogen atoms in the tertiary amine and pyridine groups (Table 4). There are additional differences between the Fe−N2 bond when compared with those from the pyridine and amino ligands, which arise primarily from the fact that the carboxamido nitrogen has two lone pairs that can interact with the metal center rather than the single lone pair on the other non-NO nitrogen ligands. For example, the covalent character in the bond between Fe and the carboxamido N results from the fact that each lone pair on the non-NO nitrogen ligands contributes approximately 0.2 $|e^-|$. Visualization of NBOs and their corresponding NLMOs for the Fe−N bonds also suggests that π-donation from the pyridine and tertiary nitrogens is mostly into Fe orbitals of either $d_{x^2-y^2}$ or d_{z^2} symmetry. In the case of the carboxamido N, however, LP[37] delocalization involves the Fe−N_{NO} π bonding orbital (∼50% into Fe, ∼18% into the NO π^*, and ∼19% into C1) (Figure 3B). This interaction might be expected to strengthen the Fe−N_{NO} bond while weakening the N−O bond to some extent.

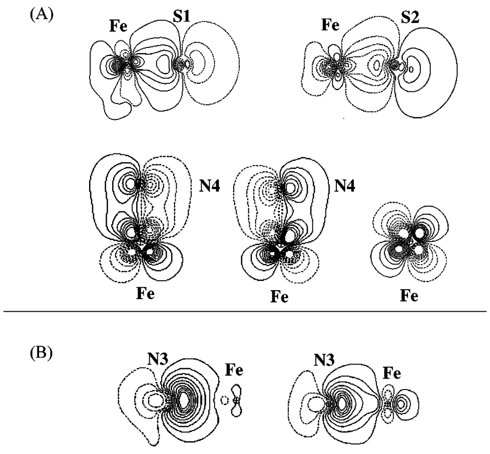

Figure 4. (A) NBOs with significant Fe character in complex **2**. (B) An NBO (left) and its corresponding NLMO (right) that show ligand-to-metal σ donation between a non-NO nitrogen donor and Fe in complex **2**. Atom labels, which indicate the nuclei associated with the electrons in the MO, correspond to those shown in Figure 2, and all contour plots were generated with NBOView 1.0 using a value of 0.03.[43]

Even though there is a mixed coordination of sulfur and nitrogen ligands about the metal, NBO analysis of complex **2** suggests that the bonding interaction between NO and the Fe-center is very similar in terms of symmetry and bond order to that computed for complex **1**. Hence, the Fe−NO bond in **2** has significant double bond character, as indicated by calculated NLMO/NPA and NBO bond orders of 1.351 and 1.370 (Table 3), respectively, and the bonding is of π symmetry (Figure 4A) consisting of ∼60% Fe and 30% NO π^* character (Table S1). The presence of three doubly occupied NBOs on Fe and an unoccupied π^* NBO in the NO moiety indicates that complex **2** is best regarded as an Fe(II)−NO^+ system, in a manner similar to complex **1**. On the other hand, the presence of the thiolate ligands does appear to change the symmetry of the Fe d orbitals that interact with NO. Hence the Fe−N_{NO} bonding involves Fe NBOs that are mainly composed of d_{xz} and d_{z^2} NHOs rather than the d_{yz} and d_{xz} NHOs employed in complex **1** (Table S1). This difference arises from the fact that the Fe d_{yz} NHO in complex **2** is the main Fe orbital involved in binding the thiolate ligand (S2) trans to the NO (Figure 2). This finding is especially intriguing, because it has been hypothesized that the presence of a thiolate ligand trans to NO is important in modulating the photolability of the Fe−NO bond.[4a] Examination of the other Fe−S bond in the complex, which is cis to the NO moiety, suggests that chemical bonding occurs via overlap of mainly Fe d_{xy} and S p_y NHOs (Figure 4B). Both ground-state Fe−S bonds are, however, of similar bond order (Table 3) and the same σ-type symmetry (Table S1). The high degree of covalency in the bonds between Fe and the thiolate ligands in **2** also impacts the composition of the Fe NHOs compared to those in complex **1**. For example, although there is still one occupied LP-type NBO that is of

---

(37) We, and the NBO program authors,[27] define a "lone pair", symbolized here by LP, to be a doubly occupied NBO that is not involved in bonding, i.e., a valence orbital that is localized to a single atomic center. In the case of complex **3**, however, the maximum possible spin−orbital occupancy of an LP has a value of 1.0.[25]

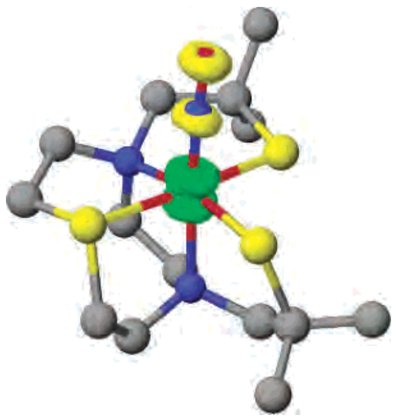

Figure 5. Graphical representation of the B3LYP spin magnetization density for the BLZYP-optimized structure of $\{Fe{-}NO\}^6$ complex **3**. Positive density is contoured as green, negative as yellow. For clarity, we show only non-hydrogen atoms, which are colored using the following scheme: C, black; N, blue; O, red; S, yellow; Fe, orange. This image was generated using the CAChe Worksystem Pro V6.0 software package.[42]

mostly Fe d_{xy} character, all of the Fe NHOs are involved in bonding with the NO or the thiolate ligands (Figure 4A). The Fe NBOs also gain occupancy via charge-transfer from the non-NO nitrogen atoms, giving small calculated covalencies in the approximate range of 0.1−0.2 $|e^-|$ (Figure 4B). The Fe−N2 bond that is trans to S1 (Figure 2) is formed by σ-donation to the metal (Figure 4B) and exhibits the least amount of covalent bonding. In this, and other respects, we note that the Fe−N2 bond in **2** is similar in nature to the bonds between Fe and the non-NO nitrogen ligands calculated for complex **1**.

Spin-restricted and spin-unrestricted single-point B3LYP calculations were performed for complex **3** at its gas-phase BLYP-optimized geometry. The unrestricted B3LYP energy was 1053 cm^{-1} lower than that determined in the spin-restricted calculation, and therefore, the unrestricted B3LYP density matrix was used in our NBO analysis of the chemical bonding. A small amount of spin contamination, as indicated by an $\langle S^2\rangle_{KS}$ value of 0.047, was present, however, and visualization of the spin-magnetization density of the Kohn−Sham wave function revealed unpaired α and β spin densities on Fe and NO, respectively (Figure 5). As noted above, $\{Fe{-}NO\}^6$ complex **3** exhibits no Fe−NO photolability under conditions that result in NO release from complexes **1** and **2**.[13a,13b] While we have detailed the strengths and limitations of employing single-determinant Kohn−Sham descriptions of Fe-containing complexes in understanding the chemical bonding elsewhere,[25] NBO analysis of the unrestricted B3LYP density matrix showed some interesting differences in the bonding description for this complex when compared with **1** and **2**. For example, the NPA/NLMO and NBO bond orders calculated for the $Fe{-}N_{NO}$ bond in complex **3** are 1.175 and 1.020, respectively, suggesting that there is less double bond character than for the cognate $Fe{-}N_{NO}$ bonds in the other two complexes (Table 3). In addition, the Fe character in the $Fe{-}N_{NO}$ bonding NBO is only approximately 46%. An analysis of the NBOs and NLMOs involved in $Fe{-}N_{NO}$ bond for complex **3** suggests that there is one $Fe{-}N_{NO}$ NBO that is doubly occupied, due to paired α- and β-electrons, and one singly occupied β $Fe{-}N_{NO}$ NBO (Figure 6). This should be contrasted with complexes **1** and **2** in which two doubly occupied NBOs were evident in the calculations. Another difference in the $Fe{-}N_{NO}$ bonding of complex **3** seems to be the contribution of metal-to-ligand π-donation of an unpaired α electron from the Fe d_{yz} NBO into the NO π^* NBO (Figure 6D). We note that the $Fe{-}N_{NO}$ π^* antibonding NBO in complex **3** has an average occupancy of only about 0.3 $|e^-|$, in contrast to the occupancies of ~0.6 $|e^-|$ calculated for complexes **1** and **2** (Table S1). The extent of spin contamination is small, however, and inspection of the NBOs indicates that there are three electron pairs in the Fe NBOs and a π^* NBO on the NO ligand that has low occupancy (0.025). We therefore suggest that this complex may be best described as Fe(II)−NO^+, albeit with a small contribution from the Fe(III)−NO• form. Inspection of the NBOs indicated distinct differences between the Fe−S bonds involving either the neutral thioether (S1) or the thiolate (S2 and S3) ligands. For example, the calculated bond covalencies of the Fe−S2 and Fe−S3 bonds were 1.06 $|e^-|$ and 1.11 $|e^-|$, respectively, compared to 0.18 $|e^-|$ for the Fe−S1 bond (Table 4). The small amount of covalency in the bond between Fe and the thioether is associated with ligand−metal σ-donation. Only σ-bonds involving the thiolate ligands were sufficiently covalent to give rise to Fe−S bonding NBOs, the interaction between the metal and the two thiolates involving the Fe d_{xy} and d_{z^2} NHOs and the S p_x and p_y NHOs (Figure 7A). Finally, the extent of covalency in the Fe−N bonds involving the

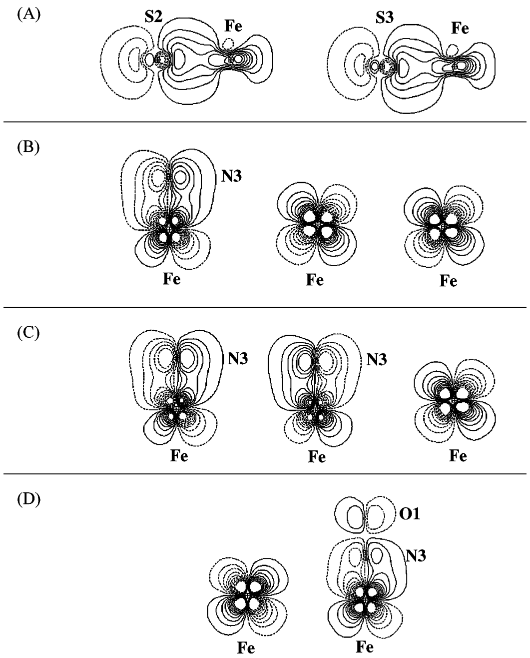

Figure 6. NBOs with significant Fe character in complex **3** corresponding to (A) Fe−S bonding within the β NBO basis, (B) $Fe{-}N_{NO}$ bonding and Fe LPs within the β NBO basis, and (C) $Fe{-}N_{NO}$ bonding and Fe lone pairs within the β NBO basis. Note that Fe−S bonding in the NBO basis is similar to that shown in Figure 6A. (D) An NBO (left) and its corresponding NLMO (right) illustrating Fe-to-NO π back-bonding in complex **3**. Atom labels, which indicate the nuclei associated with the electrons in the MO, correspond to those shown in Figure 2, and all contour plots were generated with NBOView 1.0 using a value of 0.03.[41]

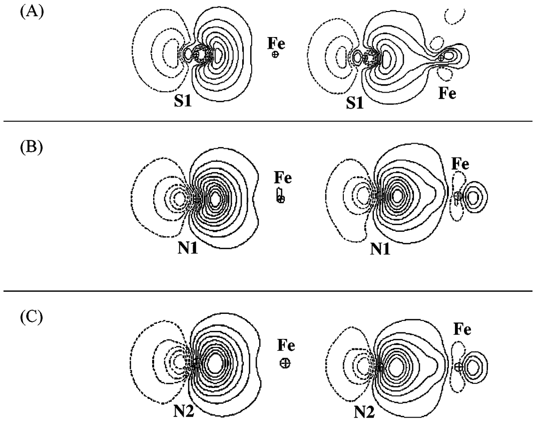

Figure 7. Selected NBOs (left) and their corresponding NLMOs (right) in complex **3** showing ligand-to-metal σ donation for non-NO ligands. (A) Fe−S1 bonding. (B) Fe−N1 bonding. (C) Fe−N2 bonding. Atom labels, which indicate the nuclei associated with the electrons in the MO, correspond to those shown in Figure 2, and all contour plots were generated with NBOView 1.0 using a value of 0.03.[43]

non-NO ligands arises from ligand−metal σ-donation and is similar to that observed for similar interactions present in complexes **1** and **2** (Figure 7).

UV/Visible Spectroscopy of Complexes 1−3. With the availability of BLYP-optimized structures for the {Fe−NO}^{6} complexes, we undertook to compute their in vacuo spectroscopic properties. In all three cases, we performed an RHF SCF calculation to identify configurations located within 50 000 cm^{-1} of the ground state. The results of this initial computation were then used to obtain the relevant MOs used in subsequent CIS calculations. This procedure avoids artifacts arising from active spaces that are too large for use within this modified zero differential overlap model.[32] Thus, the theoretical INDO/S UV/visible spectrum for complex **1** (Figure 8A) was computed using a CI that included all single excitations from the 10 highest energy occupied MOs into the 10 lowest energy unoccupied MOs. We note that the HOMO and HOMO−1 in these INDO/S calculations corresponded to nonbonding MOs on the carboxamido moiety, and the two Fe−NO π^* MOs were the LUMO and LUMO+1. These semiempirical MOs are qualitatively similar to the Kohn−Sham orbitals computed using the B3LYP functional. The theoretical spectrum computed for complex **1** contained two absorption maxima at 415 and 680 nm and a shoulder at 550 nm (Figure 8A). The experimental spectrum for complex **1** exhibits absorption maxima at wavelengths of 365 and 500 nm, with absorptivities of 1040 and 1840 M^{-1} cm^{-1}, respectively.[10] While we did observe absorption features in the calculated spectrum of **1** at 360 and 470 nm, which are close to the most intense experimental peaks in this region, the theoretical oscillator strengths for these signals were lower than those associated with transitions of greater oscillator strength calculated at 415 and 680 nm. In the absence of experimental assignments, which have not yet been reported for any of these three {FeNO}^{6} complexes, we have examined the nature of the electronic transitions as predicted within the INDO/S semiempirical model. These studies reveal the UV/visible spectrum to be dominated by ligand-to-metal charge-transfer (LMCT) transitions, many of which involve electron transfer from the nonbonding MO associated with the carboxamido group (Table 5). For example, the peak at 680 nm arises from LMCT in which an electron is promoted from a MO composed primarily of nonbonding p orbitals associated with the oxygen and nitrogen atoms in the carboxamido moiety into the Fe−NO π^* antibonding MO (Figure 8B). The calculated transitions at 470 and 360 nm involve electronic promotions from the two nonbonding MOs associated with the deprotonated amide into the Fe d_{z^2} MO and into the Fe−NO π^* antibonding MO, respectively (Table 5). The transition at 415 nm, the largest calculated oscillator strength in the visible region, also corresponds to promotion of an electron into the Fe−NO π^* antibonding MO from the carboxamido group. Hence, these visible-region transitions might be expected to decrease the Fe−N$_{NO}$ bond order in the excited state, thereby increasing the likelihood of photodissociation. These theoretical observations are consistent with the hypothesis that ligation of the metal by the deprotonated amide underpins the observed photolability of complex **1**.[10] The shoulder at 550 nm in the theoretical spectrum corresponds to a transition of mostly dd* character from the Fe d_{yz} MO into the Fe d_{z^2} MO. High-energy transitions (λ < 300 nm) having large oscillator strengths were present in the theoretical spectrum, but these absorption features appear to be associated primarily with $\pi-\pi^*$ transitions that occur within the pyridine moieties coordinating the metal.

Similar calculations on complex **2**, at its BLYP-optimized geometry, employed an active space comprising eight occupied and six virtual MOs centered about the HOMO and LUMO. In contrast to our observations for **1**, the occupied frontier MOs were composed primarily of either Fe−S σ bonding or nonbonding MOs on the thiolate ligands, although the INDO/S LUMO and LUMO+1 MOs still corresponded to the Fe−NO π^* antibonding orbitals. The theoretical UV/visible spectrum calculated for complex **2** was in reasonable agreement with experimental measurements (Figure 8C). For example, the single absorption feature observed at 420 nm was comparable to that calculated using the INDO/S CIS method to have a value of 412 nm. A more detailed analysis of the INDO/S calculation suggested that the absorption features were dominated by LMCT transitions from thiolate nonbonding and Fe−S bonding MOs into either the Fe−NO π^* MO or Fe d orbitals. Thus, the transition at 412 nm could be assigned as resulting from promotion of an electron into the Fe−NO π^* MO from an orbital for which a significant component is the Fe−S2 σ bond (Figure 8D). We would therefore expect this transition to weaken both the Fe−S and Fe−NO bonds. A calculated absorption feature with significant oscillator strength at 390 nm appears to be associated with two energetically degenerate transitions. The first of these is a MLCT transition from an MO composed mostly of Fe d_{z^2} and Fe d_{xz} orbitals into the NO π^* MO, while the second transition is a transition in which electronic promotion takes place from an MO that has mostly Fe d_{xy} character into an MO having predominantly Fe−S2 σ^* character. Another interesting aspect of this analysis is that

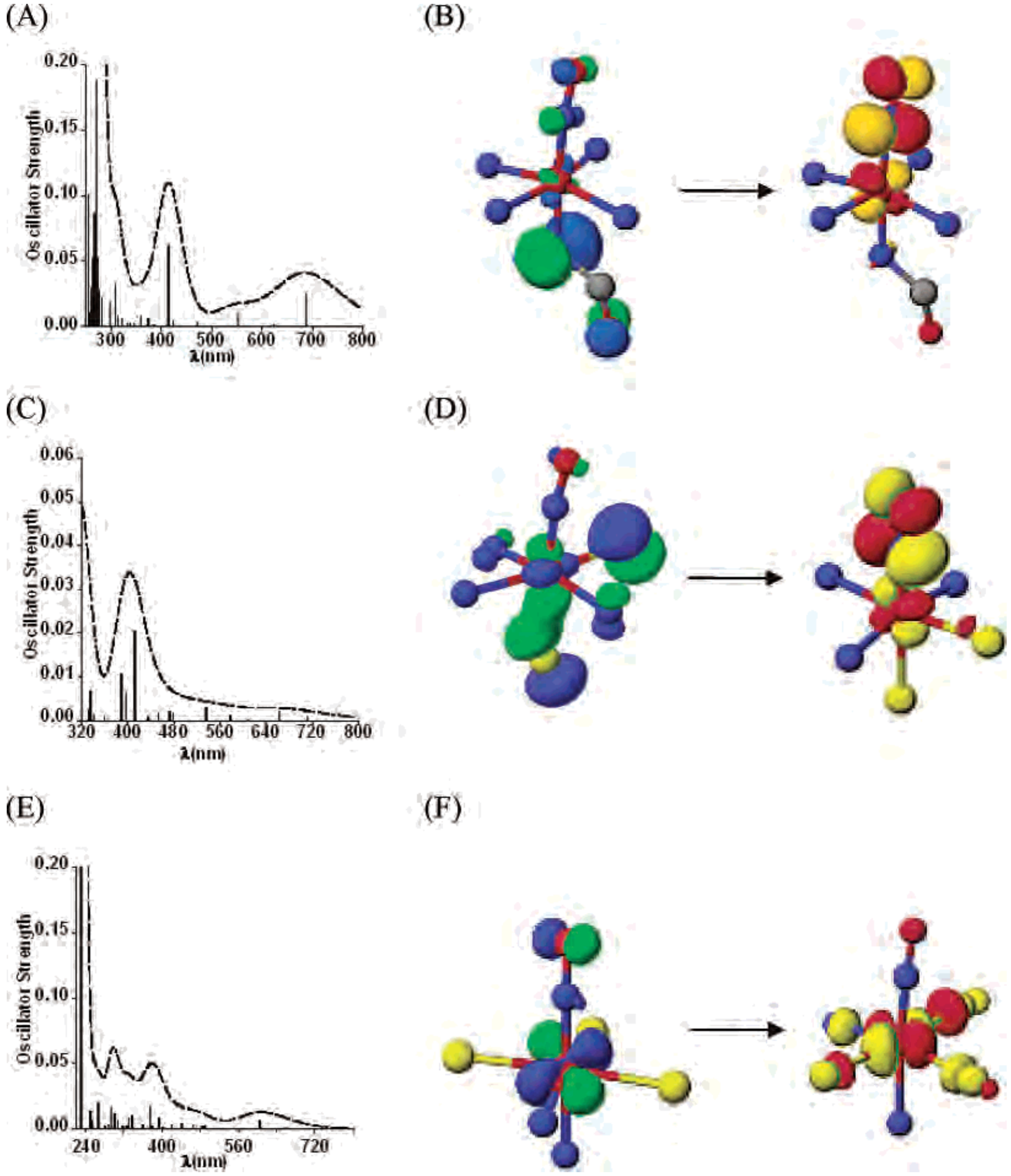

Figure 8. Simulated UV/visible spectra of {Fe−NO}^{6} complexes **1**−**3** at their BLYP-optimized geometries. (A) In vacuo INDO/S CIS spectrum calculated for complex **1**. (B) Graphical representation of the electronic transition calculated for the 680 nm photoexcitation of **1**. The phases of the initial (left) and final (right) MOs involved in promotion of the electron are shown in blue/green and red/yellow, respectively. Non-hydrogen atoms are colored using the following scheme: C, black; N, blue; O, red; S, yellow; Fe, orange. (C) In vacuo INDO/S CIS spectrum calculated for complex **2**. (D) Graphical representation of the electronic transition calculated for the 410 nm photoexcitation of **2**. Atom and orbital coloring is identical to that in Figure 8B. (E) In vacuo INDO/S CIS spectrum calculated for complex **3**. (F) Graphical representation of the electronic transition calculated for the 658 nm photoexcitation of **3**. Atom and orbital coloring is identical to that in Figure 8B. In all simulated spectra, vertical lines show the theoretical absorption maxima, and their length is proportional to calculated oscillator strength. The dashed lines represent a fit to Gaussian functions with bandwidths of 3200 cm^{-1}, normalized to the height of the highest energy transition.

both thiolate ligands are equally involved in transitions that promote an electron into the Fe−NO π^* MO, and hence these calculations do not provide strong support for the hypothesis that a trans thiolate is necessary for photolability of the Fe−N$_{NO}$ bond. We also note that these INDO/S CIS gas-phase calculations predict low-intensity, low-energy transitions at 662 and 710 nm that have not been reported experimentally. These both correspond to transitions from nonbonding p orbitals on sulfur into the Fe−NO π^* MO.

Calculations on Fe-nitrosyl complex **3** employed a smaller active space comprising 10 occupied and five virtual MOs centered about the HOMO and LUMO. In the INDO/S wave function describing complex **3**, the frontier occupied MOs correspond to nonbonding MOs located on the thiolate ligands and Fe−S σ bonding MOs. Once again, the experimental and calculated spectra for this complex were reasonably similar. For example, the computed transitions at 604 and 658 nm correspond to experimental absorption features at 535 and 649 nm, respectively (Figure 8E). Unlike the low-energy transitions of the photolabile {FeNO}^{6} complexes **1** and **2**, however, the calculated absorptions at 604 and 658 nm for complex **3** do not excite an electron into the Fe−NO antibonding orbital. Instead they appear to be dd* in nature with some intensity borrowing from transitions of CT

Table 5. In Vacuo INDO/S CIS Electronic Excitations Calculated for {Fe−NO}^{6} Complexes **1**−**3** at Their BLYP-Optimized Ground-State Geometries[a]

E_{calc}	type	theoretical (INDO/S) assignment[b]	E_{obs}
		Complex **1**	
14 536 (0.025)[c]	LMCT	amide nb → Fe−NO π*	
18 125 (0.010)	dd*	$d_{yz} \rightarrow d_{z^2}$	
21 242 (0.003)	LMCT	amide nb → d_{z^2}	20 000 (1040)[d]
23 682 (0.004)	LMCT	amide nb → Fe−NO π*	23 809 (1700)
	CT	d_{yz} → NO π*	
24 123 (0.061)	LMCT	amide nb → Fe−NO π*	
26 747 (0.006)	CT	Fe−NO π bd → $d_{x^2-y^2}$	
27 813 (0.008)	LMCT	amide nb → Fe−NO π*	27 397 (1840)
30 993 (0.006)	LMCT	amide nb → Fe−NO π*	
	LMCT	pyridine N1 → Fe−NO π*	
32 367 (0.032)	LMCT	amide nb → d_{z^2}	
		Complex **2**	
14 079 (0.0009)	LMCT	S1, S2 nb → Fe−NO π*	
15 100 (0.002)	LMCT	S1, S2 nb → Fe−NO π*	
	LMCT	S1, S2 nb → d_{z^2}	
18 678 (0.003)	LMCT	S1, S2 nb → Fe−NO π*	
24 290 (0.020)	LMCT	S2 σ bd → Fe−NO π*	23 809 (1700)
	LMCT	S1, S2 nb → Fe−NO π	
25 273 (0.006)	LMCT	S1, S2 nb → Fe−S2 σ*	
25 746 (0.011)	CT	d_{z^2} → NO π*	
	CT	dxy → Fe−S2 σ*	
29 900 (0.006)	LMCT	Fe−S2 σ bd → Fe−NO π*	
31 511 (0.016)	LMCT	Fe−S2 σ bd → Fe−NO π*	
	LMCT	S1, S2 nb → Fe−NO π*	
31 649 (0.030)	LMCT	Fe−S2 σ bd → d_{z^2}	
		Complex **3**	
15 187 (0.0009)	dd*	$d_{xy} \rightarrow d_{xz}$	15 408[e]
16 552 (0.007)	dd*	$d_{z^2} \rightarrow d_{x^2-y^2}$	
20 429 (0.002)	CT	d_{xy} → NO π*	18 692[e]
21 544 (0.002)	CT	d_{yz} → NO π*	
22 731 (0.003)	LMCT	S2 nb → NO π*	
23 857 (0.003)	dd*	$d_{xy} \rightarrow d_{x^2-y^2}$	
	LMCT	S3 nb → Fe−NO π*	
26 681 (0.017)	LMCT	Fe−S3 σ bd → Fe−NO π*	
	CT	d_{yz} → NO π*	
29 671 (0.010)	LMCT	Fe−S3 σ bd → Fe−NO π*	
30 446 (0.008)	LMCT	Fe−S3 σ bd → Fe−NO π*	
32 665 (0.006)	CT	Fe−S3 σ bd → Fe−NO π*	
33 312 (0.011)	LMCT	d_{xy} → NO π*	33 333[e]

[a] Atom labels correspond to those shown in Figure 2. [b] Amide refers to the carboxamido ligand in complex **1**, bd and nb indicate bonding and nonbonding MOs, respectively. [c] All energies are reported in units of cm^{-1}. Values in parentheses correspond to calculated oscillator strength. [d] All energies are reported in units of cm^{-1}. Values in parentheses correspond to observed extinction coefficients (M^{-1} cm^{-1}). [e] Extinction coefficients are not available for these absorption features.

character (Figure 8F). In contrast to complexes **1** and **2**, the transitions computed for complex **3** appear more equally divided into CT type transitions, in which the electron moves from a nonbonding Fe MO into the Fe−NO π* MO, and LMCT transitions originating from the thiolate ligands (Table 5). For example, the absorption calculated at approximately 300 nm can be assigned as an Fe^{2+} → NO^{+} CT transition. It is likely that such CT type transitions will serve to change the Fe(II)−NO^{+} bond to a configuration more like [Fe(III)−NO•]. Studies of nitroprusside have shown that similar transitions also result in metastable states.[38]

We were concerned by the possibility that important effects arising from the solvent environment had not been modeled by these in vacuo studies and therefore carried out INDO/S-SCRF calculations in which a continuum solvation model was employed to determine the extent and nature of solvatochromic shifts (Figure 9).[33,39] SCRF parameters were chosen for each complex to reflect the properties of the solvent used in determining its experimental UV/visible spectrum. Hence, the electronic spectrum of complex **1** in the solvent field was computed using values of 37.5 and 1.3441 for the dielectric constant (ϵ) and refractive index (η) of acetonitrile, respectively (Figure 9A). Inclusion of the solvent environment did shift the absorption maxima calculated for complex **1**, thereby increasing the agreement of the theoretical and experimental spectra. For example, the gas-phase transitions at 680, 410, and 360 nm were shifted to 660, 400, and 380 nm, respectively. The most important aspect of these calculations, however, was that inclusion of solvation effects did not change the qualitative nature of the MOs involved in the electronic excitations associated with these peaks. Hence, the 660 nm transition still arose from promotion of an electron into the Fe−NO π* MO, and LMCT from the carboxamide moiety remained a dominant feature of the photochemical excitation of the "solvated" Fe−nitrosyl complex **1**.

In the case of complex **2**, the inclusion of the SCRF to represent acetonitrile gave a spectrum that exhibited only small solvatochromic shifts from that calculated for the in vacuo system (Figure 9B), although the relative intensities of the two transitions at approximately 390 and 410 nm were reversed in the INDO/S-SCRF CIS spectrum. Closer examination suggested that while the 410 nm transition in the gas phase spectrum was associated almost completely with LMCT transitions from ligated S MOs into the Fe−NO π* MO, the SCRF apparently lowers the relative intensity of the cognate absorption feature at 406 nm by altering the composition of MOs involved in the electronic excitation. Thus, while this peak still arises partly from a transition from the Fe−S σ bonding MO/S1 nonbonding MO into the Fe−NO π* antibonding MO, the excitation is also composed of transitions from the Fe−NO π bonding MO into the Fe $d_{x^2-y^2}$ orbital. On the other hand, although the assignments for the 406 and 410 nm absorptions differ slightly in composition in the INDO/S-SCRF and in vacuo INDO/S models, respectively, both transitions will have the effect of weakening the Fe−N$_{\text{NO}}$ bond. This observation is therefore consistent with the observed photochemical behavior of this complex.[11] The transition at 390 nm computed using the INDO/S-SCRF method is degenerate, being primarily composed of a CT transition from the Fe d_{z^2} MO into the NO π* MO, as seen for the in vacuo calculation. On the other hand, this transition in the INDO/S-SCRF calculation appears to be degenerate with electronic excitations from the nonbonding orbitals on S1 and S2 into the Fe−NO π* MO. Weak, low-energy absorptions are also calculated at 660 and 700 nm, but the nature of these transitions is unchanged upon addition of the SCRF.

---

(38) Buchs, M.; Daul, C. A.; Manoharan, P. T.; Schläpfer, C. W. *Int. J. Quantum Chem.* **2003**, *91*, 418−431.

(39) (a) Cramer, C. J.; Truhlar, D. G. *Chem. Rev.* **1999**, *99*, 2161−2200. (b) Tomasi, J.; Persico, M. *Chem. Rev.* **1994**, *94*, 2027−2094.

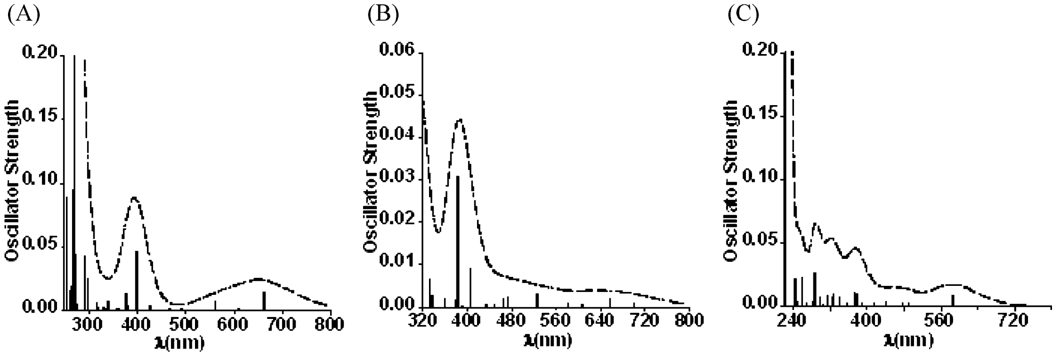

Figure 9. Simulated solution-phase UV/visible spectra of $\{Fe-NO\}^6$ complexes **1**−**3** at their BLYP-optimized geometries. (A) INDO/S-SCRF CIS spectrum calculated for complex **1**. (B) INDO/S-SCRF CIS spectrum calculated for complex **2**. (C) INDO/S-SCRF CIS spectrum calculated for complex **3**. Vertical lines show the theoretical absorption maxima, and their length is proportional to calculated oscillator strength. The dashed lines represent a fit to Gaussian functions with bandwidths of 3200 cm^{-1}, normalized to the height of the highest energy transition.

Our final set of INDO/S-SCRF calculations examined the effects of DMF solvation ($\epsilon = 36.7$, $\eta = 1.43$) on the calculated transition energies and assignments for $\{Fe-NO\}^6$ complex **3** (Figure 9C). In this case, the semiempirical model predicted two low-energy transitions at 657 and 586 nm, in slightly better agreement with experiment than seen in the in vacuo calculations on this complex. Both of these absorptions were assigned as dd* coupled with CT-type transitions involving the Fe−S σ bonding MOs. The calculated absorption feature at 290 nm corresponds to the solvent-shifted peak observed at approximately 300 nm in the in vacuo INDO/S spectrum and can be assigned to a LMCT from S nonbonding p orbitals into MOs composed primarily of the Fe 3d orbitals, again as for the gas-phase transition. Finally, we note that the number of CT transitions in which electronic excitation takes place from nonbonding Fe d orbitals into the NO π^* MO is approximately equal to that for transitions from the metal ligands into the Fe−NO π^* MO. Hence, the inclusion of the reaction field arising from the DMF solvent does not fundamentally affect the conclusions of the in vacuo calculations, i.e., that (i) there are no low-energy absorptions that result in the promotion of an electron from Fe d and Fe−S σ bonding MOs into the Fe−NO π^* antibonding Mos, as seen for both complexes **1** and **2**, and (ii) many of the transitions will merely create an [Fe(III)−NO•] system.

Summary

We have calculated both the ground- and excited-state properties of three $\{Fe-NO\}^6$ complexes that exhibit distinct behavior with respect to light-activated NO release. Our results suggest that the majority of and most intense transitions for the mononuclear, photolabile complexes **1** and **2** correspond to promotion of an electron into the Fe−NO π^* antibonding MO. Furthermore, similar electronic excitations that lead to weakening of the Fe−N_{NO} bond are not the primary transitions computed for complex **3**, which does not appear to be photolabile.[13a] These conclusions are unchanged by the inclusion of SCRF continuum solvation models, which demonstrate that while the solvent polarizability causes shifts in the absorption maxima, the MOs that are involved in the electronic transitions remain mostly unchanged. We note, however, that time-dependent DFT (TD-DFT) methods[40] did not give calculated spectra for these $\{Fe-NO\}^6$ complexes that were in especially good agreement with experiment, and a number of the computed transitions were physically questionable (Greene, unpublished results).[41]

Our calculations also provide some insight into the correlation between metal ligands and photolability of the Fe−N_{NO} bond. For example, the INDO/S model supports the published hypothesis that the presence of the carboxamido group is necessary for the observed photodissociation of Fe−NO bond in complex **1**,[10] by providing direct information on the changes introduced into the electronic structure upon light irradiation. In a similar manner, our computational results provide evidence for the idea that the difference in photolability of complexes **2** and **3**, which lack carboxamido coordination, may be associated with the presence of a thiolate ligand trans to the nitrosyl substituent. Thus, in the absence of an axial thiolate, the most intense transitions computed for complex **3** correspond to CT in which an electron from the equatorial sulfur ligands is promoted into the Fe d orbitals rather than into the Fe−NO π^* antibonding MO.

On the basis of the results reported here, we conclude that the calculation of electronic absorption spectra for DFT-optimized structures using the computationally efficient INDO/S CIS method is an effective strategy for predicting the likely photolability of inorganic $\{Fe-NO\}^6$ complexes. These studies therefore represent a further application of our computational approach for understanding the active site Fe(III) center in NHase and strengthen our conclusions

---

(40) Bauernschmitt, R.; Ahlrichs, R. *Chem. Phys. Lett.* **1996**, *256*, 454−464.

(41) (a) Solomon, E. I.; Szilagyi, R. K.; DeBeer George, S.; Basumallick, L. *Chem. Rev.* **2004**, *104*, 419−458. (b) Deeth, R. J. *Faraday Discuss.* **2003**, *124*, 379−391. For the failure of time-dependent DFT to model large π-systems, see also: (c) Parac, M.; Grimme, S. *Chem. Phys.* **2003**, *292*, 11−21. The problems of employing this method to compute spectra for transition-metal complexes are also alluded to in the following references: (d) Fouqueau, A.; Mer, S.; Casida, M.; Max, L.; Daku, L.; Hauser, A.; Neese, F. *J. Chem. Phys.* **2004**, *120*, 9473−9486. (e) Neese, F. *J. Chem. Phys.* **2003**, *119*, 9428−9443.

(42) CAChe Group, Fujitsu America, Inc., Beaverton, OR (www.cachesoft-ware.com).

(43) Wendt, M.; Weinhold, F. *NBOView 1.0*. Theoretical Chemistry Institute, University of Wisconsin: Madison, WI, 2001.

concerning the likely role of post-translational modification in modulating the photochemical regulation of the enzyme.[14]

Acknowledgment. We thank the National Science Foundation (CHE-0079008) for support of this work and the National Partnership for Advanced Computational Infrastructure (NPACI) for the provision of supercomputing facilities. We also acknowledge Dr. Craig Grapperhaus (University of Louisville) for providing unpublished details concerning the UV/visible absorption spectrum of complex **3**, Dr. Christopher Chang and an anonymous reviewer for insightful comments concerning the manuscript, and Dr. Marshall Cory, Jr., for developing the software used to perform Gaussian fitting of the calculated electronic transitions.

Supporting Information Available: Calculations showing the effect of crystal packing on the observed structure of **1** and the tabulated NHO compositions of selected NBOs in complexes **1**−**3** at their BLYP-optimized geometries. This material is available free of charge via the Internet at http://pubs.acs.org.

IC0499695